



Iron-impregnated zeolite catalyst for efficient removal of micropollutants at very low concentration from Meurthe river

Hawraa Ayoub^{1,2} · Thibault Roques-Carmes¹ · Olivier Potier¹ · Bachar Koubaissy² · Steve Pontvianne¹ · Audrey Lenouvel³ · Cédric Guignard³ · Emmanuel Mousset¹ · Hélène Poirot¹ · Joumana Toufaily² · Tayssir Hamieh²

Received: 15 August 2017 / Accepted: 2 January 2018 / Published online: 11 January 2018
© Springer-Verlag GmbH Germany, part of Springer Nature 2018

Abstract

In this paper, for the first time, faujasite Y zeolite impregnated with iron (III) was employed as a catalyst to remove a real cocktail of micropollutants inside real water samples from the Meurthe river by the means of the heterogeneous photo-Fenton process. The catalyst was prepared by the wet impregnation method using iron (III) nitrate nonahydrate as iron precursor. First, an optimization of the process parameters was conducted using phenol as model macro-pollutant. The hydrogen peroxide concentration, the light wavelength (UV and visible) and intensity, the iron loading immobilized, as well as the pH of the solution were investigated. Complete photo-Fenton degradation of the contaminant was achieved using faujasite containing 20 wt.% of iron, under UV light, and in the presence of 0.007 mol/L of H₂O₂ at pH 5.5. In a second step, the optimized process was used with real water samples from the Meurthe river. Twenty-one micropollutants (endocrine disruptors, pharmaceuticals, personal care products, and perfluorinated compounds) including 17 pharmaceutical compounds were specifically targeted, detected, and quantified. All the initial concentrations remained in the range of nanogram per liter (0.8–88 ng/L). The majority of the micropollutants had a large affinity for the surface of the iron-impregnated faujasite. Our results emphasized the very good efficiency of the photo-Fenton process with a cocktail of a minimum of 21 micropollutants. Except for sulfamethoxazole and PFOA, the concentrations of all the other microcontaminants (bisphenol A, carbamazepine, carbamazepine-10,11-epoxide, clarithromycin, diclofenac, estrone, ibuprofen, ketoprofen, lidocaine, naproxen, PFOS, triclosan, etc.) became lower than the limit of quantification of the LC-MS/MS after 30 min or 6 h of photo-Fenton treatment depending on their initial concentrations. The photo-Fenton degradation of PFOA can be neglected. The photo-Fenton degradation of sulfamethoxazole obeys first-order kinetics in the presence of the cocktail of the other micropollutants.

Keywords Photo-Fenton · Wastewater treatment · Micropollutants · Pharmaceuticals · Iron-impregnated faujasite · Phenol · Emerging contaminants

Responsible editor: Vítor Pais Vilar

Electronic supplementary material The online version of this article (<https://doi.org/10.1007/s11356-018-1214-0>) contains supplementary material, which is available to authorized users.

✉ Thibault Roques-Carmes
thibault.roques-carmes@univ-lorraine.fr

¹ Laboratoire Réactions et Génie des Procédés (LRGP), UMR CNRS 7274, Université de Lorraine, 1 rue Grandville, 54001 Nancy, France

² Laboratory of Materials, Catalysis, Environment and Analytical Methods, Faculty of Sciences I, Lebanese University, Campus Rafic Hariri, Beirut, Lebanon

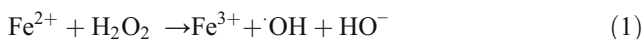
³ Luxembourg Institute of Science and Technology (LIST), 41 rue du Brill, 4422 Belvaux, Luxembourg

Introduction

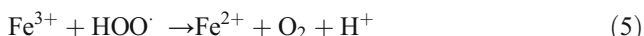
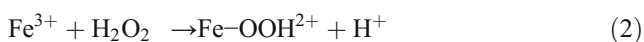
Numerous contaminants, e.g., endocrine disruptors, pharmaceuticals, and personal care products, have been detected in the outlet of conventional wastewater treatment plant (WWTP) at a trace level, i.e., in the range of nanogram per liter to microgram per liter (Fatta-Kassinos et al. 2011; Igos et al. 2012; Richardson and Kimura 2016). Even at such low concentrations, many studies highlight the potential toxicity of these micropollutants for the environment and the human health (Kovalova et al. 2013; Mariangela et al. 2013; Trapido et al. 2014). Being bio-recalcitrant, most of these emerging pollutants cannot be totally eliminated by conventional biological treatment (Rodriguez et al. 2011). Therefore, the development of an advanced physico-chemical complementary treatment becomes a promising

alternative. Advanced oxidation processes (AOPs) have been proposed as they rely on the production of very strong oxidizing agent such as hydroxyl radicals ($\cdot\text{OH}$) having a high standard reduction potential ($E^\circ = 2.80 \text{ V vs SHE}$), second only after fluorine that is ruled out for this application (de Witte et al. 2011; Ghatak 2014; Oturan and Aaron 2014). Among these nascent technologies, photo-Fenton depicted high removal rates and yields of xenobiotic pollutants, thanks to the formation of $\cdot\text{OH}$ through Fenton and Fenton-like reactions from initial addition of hydrogen peroxide (H_2O_2) with ferrous ion (Fe^{2+}) and ferric ions (Fe^{3+}) in the effluent (Hartmann et al. 2010; Xavier et al. 2016):

Fenton:

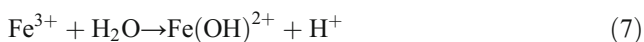


Fenton-like:



Two additional $\cdot\text{OH}$ sources can be obtained through (a) the photolysis of iron-hydroxy complexes such as $\text{Fe}(\text{OH})^{2+}$, the predominant Fe(III) species at pH 3 (Eq. (8)) and (b) the photolysis of H_2O_2 under UVA irradiation (Eq. (9)) (Loaiza-Ambuludi et al. 2014; Xavier et al. 2016):

Photo-Fenton:



However, homogeneous photo-Fenton process has been proven to have several disadvantages. This process leads to formation of sludge containing Fe ions costly removed at the end of wastewater treatment and needs a large amount of chemicals (Feng et al. 2003). Moreover, the need to continuously adjust to acidic pH (around pH 3) makes photo-Fenton process not convenient enough to be operated for wastewater application. These drawbacks limit the use of homogeneous photo-Fenton reaction in wastewater treatment. The development of heterogeneous photo-Fenton is being considered to face this issue (Nidheesh 2015). For these purposes, many supports, such as nafion, zeolite, silica, clay, and activated carbon, have been suggested in heterogeneous Fenton oxidation processes (Kim et al. 2015). Several factors, such as pore volume, pore size distribution, surface area, effectiveness, and cost, play a role in choosing the appropriate material to be used as a support (Blanco et al. 2014). Most of the suggested materials have low effectiveness or high cost. Activated

carbon, one of the most studied heterogeneous catalysts, is limited by its high cost and sludge formation (Arimi 2017). The use of zeo-type catalysts is very promising due to their unique properties (Kasiri et al. 2008) and less severe experimental conditions (mild temperature and pressure) that improve the efficiency and lower the formation of by-products compared to the other advanced oxidation treatments (Neamu et al. 2004a).

Zeolites are microporous, microcrystalline aluminosilicate materials (Neamu et al. 2004b) with a three-dimensional structure and four-connected framework built from tetrahedral of $[\text{SiO}_4]^{4-}$ and $[\text{AlO}_4]^{5-}$, bonded together via the oxygen atoms. Al^{3+} can replace Si^{4+} resulting in a negatively charged framework (Blanco et al. 2014). Zeolites are capable of complexing or adsorbing small- and medium-sized organic molecules that give them an advantage over other carriers (such as clay, activated carbon, laponite, and bentonite) (Neamu et al. 2004a) due to their molecular sieve structure and unique framework that generates a high internal surface area. They are characterized by their temperature stability, well-defined uniform pore and crystal structure, and easy ion-exchange method (Turapan et al. 2012).

Faujasites are a type of aluminosilicate zeolites combining a three-dimensional network of accessible micropores (0.74 nm) with an organic-free synthesis (Verboekend et al. 2016). The ratio of silica to the alumina determines the type (X or Y) of the synthetic zeolite (Arimi 2017). Faujasite with Si/Al ratio lower than 1.5 corresponds to faujasite X while faujasite Y has a value higher than this value (Lutz 2014). The low Si/Al ratio of faujasite X offers a large-exchange capacity governed by the high aluminum content (Neamu et al. 2004b) making it usable as ion exchanger, molecular sieve, and adsorbent. However its usage in catalysis is limited due to the instability of its protonic form (Verboekend et al. 2016). As a result, a more stable less-acidic faujasite Y is more commonly applied in preparation of heterogeneous Fenton catalyst (Arimi 2017) due to its improved catalytic and hydrothermal stability as observed in numerous petrochemical applications (Verboekend et al. 2016). Recently, metal containing zeolites have been proven to be efficient and promising catalysts for the oxidation of different groups of organic pollutants with hydrogen peroxide (Arimi 2017; Barreca et al. 2014, 2015; Kasiri et al. 2008). More particularly, zeolite-based Fe catalysts were reported to have high degradation efficiency which could be similar as homogeneous Fe ions (Noorjahan et al. 2005).

The photo-Fenton degradation of micropollutants has been studied before, but most of the research has been conducted using synthetic waters (Huang et al. 2017; Jiang et al. 2014; Lam and Mabury 2005; Natali Sora and Fumagalli 2017) or real waters (WWTP effluents or real natural water) but spiked with solutions of model micropollutants (Klamerth et al. 2012; Sanches et al. 2016). At the same time, the concentrations of

micropollutants are generally high, i.e., from microgram per liter to milligram per liter. Only very few studies work with micropollutants in real water. For example, Miralles-Cuevas et al. (2014) have reported the photo-Fenton removal of micropollutants in real municipal effluents. They studied nine pharmaceutical micropollutants of the same family with concentrations between 20.200 $\mu\text{g/L}$ and 0.86 $\mu\text{g/L}$. In addition, the photo-Fenton degradation of some specific micropollutants, such as PFCs, has been barely evaluated due to the carbon-fluorine bond that makes them environmentally persistent (Arvaniti and Stasinakis 2015).

It appears, then, relevant to work with real water containing different families of compounds. In this article, faujasite zeolite impregnated with iron has been applied to remove a cocktail of micropollutants inside real water samples from the Meurthe river (France) by the means of the heterogeneous photo-Fenton process. These contaminants belong to four different families which are pharmaceuticals, personal care products, endocrine disruptors, and perfluorinate compounds having different chemical structures. For the first time, the detection and the removal at trace levels (range of ng/L) of a mixture of 21 micropollutants in water from a river has been achieved. Moreover, working with very low concentration of micropollutants remains an analytical challenge since most of the previous studies avoid working with these low concentrations due to the complexity of the analysis on LC-MS/MS, the high number of measurement steps, and the unavailability of the needed analytical instruments in all the laboratories. However, the removal of micropollutants at such low concentration is representative of the emerging contaminant concentration level (ng/L) encountered at the outlet of the WWTP. Consequently, the results can be directly applied in wastewater treatment plants.

This paper intends to bring new scientific and technological insights through the three following objectives: (1) manufacture a catalyst (Fe) impregnated on a sorbent (faujasite Y) and characterize the multi-functional material, (2) optimize the performance of the material in synthetic medium with a representative pollutant, e.g. phenol, by varying the main impacting operating parameters of heterogeneous photo-Fenton process, and (3) test the efficiency of the materials in the treatment of real water samples containing a real cocktail of micropollutants from the Meurthe river.

Materials and methods

Chemicals

The faujasite used in our study was an industrial zeolite supplied by the Zeolyst International. The zeolite was

dealuminated. Consequently, the ratio of Si/Al was increased until 19. Table S1 of the Supporting information shows the main characteristics of this zeolite. Iron (III) nitrate nonahydrate ($\text{Fe}(\text{NO}_3)_3 \cdot 9\text{H}_2\text{O}$) salt was purchased from Sigma Aldrich. Hydrogen peroxide (H_2O_2 , 30 or 50 wt.% aqueous) was obtained from Sigma Aldrich. Concerning the model pollutant, phenol was purchased from Merck.

Catalyst preparation

Iron-impregnated faujasite was prepared by the wet impregnation method with three different impregnation percentages: 10, 20, and 30 wt.%. For this purpose, a given amount of iron (III) nitrate nonahydrate was dissolved in 50 mL of deionized water, and 1 g of faujasite was added under continuous magnetic stirring. The obtained slurries were heated slowly to 90 °C and kept at this temperature until nearly all the water had evaporated. The wet solid obtained was then dried at 100 °C for 24 h.

The synthesis of free Fe_2O_3 particles was performed using the same procedure as for the immobilized systems but in the absence of the faujasite. To this aim, 16 mg of iron (III) nitrate nonahydrate was introduced in 80 mL of deionized water in order to have the same amount of iron than that we used to prepare the 20 wt.%-impregnated faujasite.

Catalyst characterizations

Different techniques were used to characterize the faujasite before and after the iron impregnation: scanning electron microscope (SEM) coupled with energy dispersive X-ray spectroscopy (EDS), X-ray powder diffraction (XRD), diffuse reflectance UV/visible spectroscopy, and zeta potential measurements.

The impregnated zeolites were observed with a scanning electron microscope coupled with energy dispersive X-ray spectroscopy (JEOL-JSM-6490LV) after being coated with a gold/palladium alloy deposited by low-vacuum sputter coating. Powder X-ray diffraction (XRD) measurements were recorded by means of a D8 Discover BRUKER diffractometer equipped with Cu $K\alpha$ radiation. The solid samples were scanned over 2θ range of 5° to 80° at a step size of 0.02°. The nature of the Fe species in the catalyst structure was identified by diffuse reflectance UV/Visible spectrophotometry. The absorption spectra were recorded on a UV-3600 UV/visible double beam spectrophotometer (SHIMADZU) in the 200–800 nm wavelength range. The zeta potential of the particles was determined using a Zetasizer NanoZS (Malvern) equipped with a He–Ne laser at 633 nm. The nanoparticles were dispersed in Milli-Q water and diluted in an aqueous solution of NaCl (0.01 M) adjusted to the required pH through the addition of NaOH or HCl.

Photo-Fenton reactions with model pollutant

The activity of the catalyst was studied, and the optimization of the different experimental conditions was done by using phenol as a model pollutant. The photo-Fenton tests were performed, at room temperature (20 °C), inside a glass crystallizer. On the one hand, the UV irradiation was provided by a mercury lamp (low pressure mercury arc, 18 W) emitting in the near-UV. The emission of the lamp indicated a spectral response centered at 254 nm with a half band-width of 12 nm. The lamp was positioned outside the reactor and was parallel to it. The distance between the lamp and the top of the crystallizer was 3.5 cm, while the height of the solution amounted to 2.5 cm. The incident light intensity reaching the top of the reacting suspension was equal to 10^{-6} Einstein $L^{-1} s^{-1}$. On the other hand, for the photo-Fenton tests under visible light irradiation, a different lamp was employed. The source of visible light was an OmniCure® S2000 platform equipped with a 200 W lamp with an emission wavelength ranging from 250 to 500 nm. The UV emission of the lamp (below 400 nm) was filtered out by a polycarbonate plate placed between the light source and the reaction medium. The optical fiber was placed at a distance of 16.2 cm from the crystallizer containing the reaction mixture, and the height of the solution was equal to 2.5 cm. The power of the lamp was adjusted to 497 mW/cm² with 18% of light-emerging percentage.

Phenol was utilized as the representative organic pollutant because it is an aromatic compound; most of the organic micropollutants are widely present in water. The concentration of phenol studied was in milligram per liter and not in nanogram per liter because micropollutants are present in real water and most of the studies performed on phenol are in this range of concentration. Thus, it became easy to compare with the literature data to validate the results in order to optimize the process. Moreover, it was easier to analyze, quantify, and optimize the different experimental conditions using milligram per liter concentrations rather than nanogram per liter. In certain cases, the pH of the aqueous solutions was adjusted before the introduction of the catalyst through NaOH or HCl addition. For all the experiments, the catalyst (Fe/faujasite) content and the initial pollutant concentration were equal to 1 g/L and 10 mg/L, respectively. Note that depending on the nature of the light used, the size of the reactor was different but the catalyst amount/solution volume ratio was maintained constant whatever the reactor configuration. For the experiments under UV light, the photo-Fenton oxidation was carried out in solution containing 80 mg of the catalyst in 80 mL of pollutant solution. Conversely, when using visible light, 40 mg of solid catalyst was introduced inside a volume of the pollutant solution equal to 40 mL.

In a typical experiment, the dispersion containing the zeolite and the pollutant were stirred for 1 h under dark condition.

After that period, a known concentration of H₂O₂ was introduced into the suspension. The occurrence of an optimum concentration of H₂O₂ corresponding to a maximum degradation at H₂O₂ concentration between 0.01 and 0.02 M was observed experimentally in several instances (Ghaly et al. 2001; Neamu et al. 2004a; Barakat et al. 2005; Kasiri et al. 2008). Thus, the concentrations of H₂O₂ selected were below (0.0048, 0.007 M), between (0.0156 M), and above (0.06 M) this range. Just after the H₂O₂ addition, the lamp (UV or visible) was turned on. Liquid samples were taken at different time intervals. The liquid was separated from the solid by the means of 0.45 μm filters. The phenol concentration remaining in the supernatant was analyzed by both UV/Visible spectrophotometry (Cary 5G UV-Vis-NIR) at absorption wavelength of $\lambda = 269$ nm and by HPLC (Shimadzu SPD-20A UV-Vis detector) equipped with a classical C-18 column. The total organic carbon content (TOC) at the end of the experiments was measured using a TOC analyzer TOC-V_{CSH} (Shimadzu). The amount of iron species leached from the catalyst during the photo-Fenton degradation tests was measured at the end of the process using a flame atomic absorption (Thermo Electron Corporation) with a Fe lamp and standard solutions of Fe in 3 v.%-acidified HNO₃ deionized water.

It appeared important to perform blank experiments in the absence of catalyst. First, under UV light irradiation but in the absence of iron-impregnated faujasite and H₂O₂, the results indicated no photolysis of phenol (Fig. S1 of the Supporting information). Second, in the presence of UV light irradiation and H₂O₂, the degradation of phenol remains also negligible (Fig. S1 of the Supporting information).

Photo-Fenton tests with real water

Photo-Fenton tests were carried out with real water samples taken from the Meurthe river. This river was located close to Nancy in France (Fig. S2 of the Supporting information). The samplings were conducted in a site named Moulin Noir from the Meurthe river. This location was chosen in order to ensure a sufficiently large amount of micropollutants in terms of both concentration (in a range of ng/L) and nature. Twenty-one micropollutants including 17 pharmaceutical compounds were targeted. In details, bisphenol A, carbamazepine, carbamazepine-10,11-epoxide, clarithromycin, cyclophosphamide, diclofenac, erythromycin, estradiol-beta, estrone, ethynylestradiol, ibuprofen, ketoprofen, lidocaine, naproxen, PFOA, PFOS, sulfadimethoxine, sulfadimidine, sulfamethoxazole, sulfathiazole, and triclosan were specifically detected and quantified. Table S2 of the Supporting information gives more information about the 21 micropollutants.

The sampling was carried out from the middle of the bridge to ensure the good mixing of the micropollutants in water samples (Fig. S2B of the Supporting information). A glass bottle surrounded by iron cover to avoid its breakage with a

thick long ribbon was dropped from the bridge into the river to take a water sample. After sampling, the water samples were filtrated by two processes. First, funnel and filter paper were employed to remove the bulk materials. Then, the water was filtrated using successively a glass filter of 1.2 μm porosity followed by a cellulose acetate filter with a porosity of 0.45 μm . After those filtration steps, the samples of water were kept inside dark bottles in the fridge at a temperature of 4 °C.

Concerning the photo-Fenton degradation tests, 600 mL of water sample was used. This large volume was necessary for the micropollutant analysis. Actually, a final volume of 500 mL appeared necessary for the micropollutant quantification. For practical reasons, the initial volume of water was split into three crystallizers of 200 mL each in order to use the same UV lamp as described previously. For each crystallizer reactor, 0.2 g of the 20 wt.% Fe-impregnated faujasite was added into 200 mL of water. No modification of the pH or the temperature was performed. Blank experiments were undertaken. To this aim, experiments were conducted in the absence of iron-impregnated faujasite under UV illumination in the presence or in the absence of H_2O_2 . The duration of the experiments was fixed to 30 min or 6 h. To evaluate the adsorption capacity of the Fe/faujasite towards the 21 micropollutants, the suspensions were stirred for 2 h in the dark and in the absence of H_2O_2 . The photo-Fenton tests were carried out for 30 min or 6 h under UV irradiation and in the presence of hydrogen peroxide. The same experiments were performed in the dark but in the presence of H_2O_2 to evaluate the Fenton activity of the iron-impregnated faujasite. The H_2O_2 concentration was fixed to 0.007 M while the Fe/faujasite content equaled 1 g/L, unless stated otherwise. The faujasite containing 20 wt.% of iron was used as catalyst. It is also important to note that only one sampling was carried out at the end of the experiment. The treated water was centrifuged for 25 min at 4000 rpm.

For the micropollutant detection and quantification, a concentration step by Solid-Phase Extraction (SPE) was followed. The samples were filtrated under 1.2 μm glass fiber and 0.45 μm cellulose acetate filters and adjusted to pH 4 with sulfuric acid. A total of 550 mL of sample were concentrated and purified by SPE (Autotrace SPE Workstation, Thermo Fisher Scientific, Waltham, USA). The SPE cartridge (Oasis HLB 200 mg/6 mL, Waters, Milford USA) was formerly conditioned with methanol and then water at pH 4. After the sample loading, the cartridge was washed with water/methanol 95/5 (v/v), dried under nitrogen, and eluted with 10 mL of methanol. To enhance the concentration factor, the extract was evaporated under vacuum at 50 °C to the drop and recovered in 500 μL of water/methanol 90/10, the same starting conditions as those employed for the analysis. The eluents were all of ultra-pure grade. The final extract was analyzed by Liquid Chromatography (1260 Series, Agilent,

Santa Clara, USA) coupled to triple-quadrupole Mass Spectrometry (QTRAP 4500, AB Sciex, Framingham, USA). The chromatographic separation was realized on a Zorbax Eclipse Plus C18 column, 150 \times 2.1 mm ID, 3.5 μm particle size (Agilent). The flow rate of the mobile phase was kept constant at 0.25 mL/min and the oven at 40 °C. The nature of the mobile phases and the eluent programs are given in Table S3 of the Supporting information. According to the target compounds, the mass spectrometer was operated in positive or negative electrospray mode. Two transitions were saved in Multiple Reaction Monitoring mode for quantification and confirmation of each target compound. Quantitative results were provided thanks to internal calibrations.

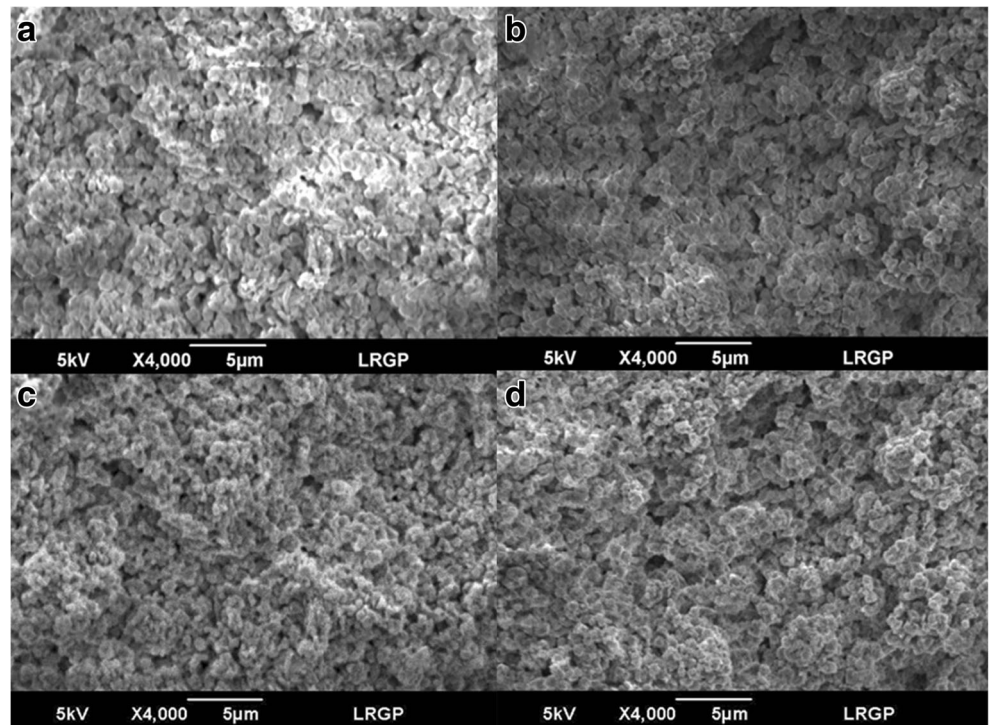
Results and discussion

Characterization of the Fe-impregnated faujasite

Figure 1 shows the SEM images of the raw and Fe-impregnated faujasite. As we can see in Fig. 1a, the raw faujasite appears as fine particles. The morphology of the faujasite is not modified by the iron impregnation. From the pictures, the possible presence of iron oxide particles (Fe_2O_3) cannot be observed. In addition, EDS is used to detect the presence of iron onto the impregnated samples (Fig. 2). For the analysis, we concentrate on the quantification of the Fe, Si, and Al elements. The amount of iron increases with the initial concentration of iron nitrate in solution. This confirms the immobilization of iron onto the zeolite for all the mixtures. The iron content is directly connected to the initial concentration of iron nitrate but is also sensitive to the zeolite amount. To estimate semi-quantitatively the amount of iron-impregnated onto the faujasite, the ratio of the atomic percentages of iron and silicon (Fe/Si) is calculated for various iron nitrate initial concentrations (Fig. 2). Note that the atomic percentage of Si is used as quantitative reference of the zeolite amount. The ratio increases continuously with the initial iron concentration.

The influence of the initial concentration of iron nitrate on the XRD patterns of the impregnated faujasite samples is depicted in Fig. 3a. The XRD pattern of the raw faujasite fits well with the one mentioned in the literature (Cejka et al. 2005; Treacy and Higgins 2007). In details, the values of the 2θ of the different peaks and their corresponding hkl indices in brackets are as follows: $2\theta = 6.19^\circ$ (111), 10.36° (220), 12.18° (311), 15.8° (331), 19.1° (511), 20.7° (440), 22.02° (420), 23.9° (533), 27.4° (642), 30.16° (660), 31.32° (555), and 32.5° (840) (Cejka et al. 2005). For all the impregnated samples, no peak corresponding to iron oxide can be detected. However, all the reflection peaks related to the faujasite are observed. Actually, in the presence of iron, the height of the peaks of the zeolite decreases in comparison to those of pure

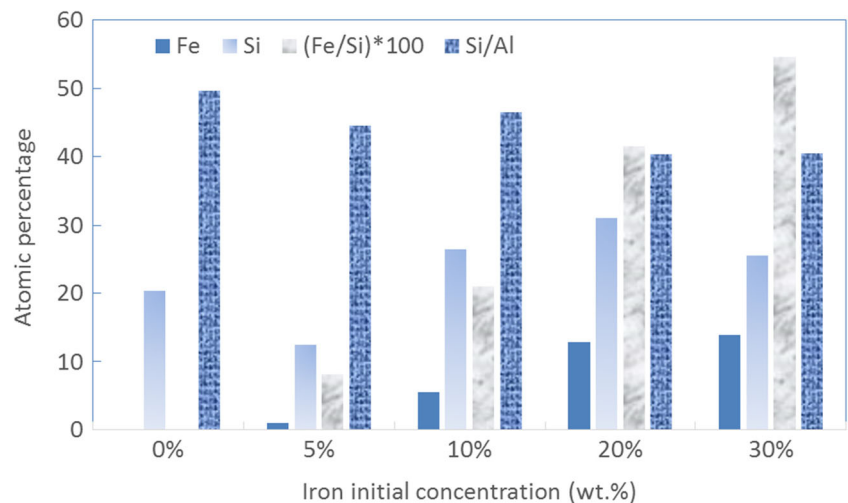
Fig. 1 SEM pictures of (a) raw faujasite and Fe-impregnated faujasite prepared with initial masses of iron (III) nitrate nonahydrate of (b) 10 wt.%, (c) 20 wt.%, and (d) 30 wt.%



faujasite. The height of the peaks diminishes with the impregnated iron content. The absence of detectable peak corresponding to iron may arise from two causes. First, this occurs when the Fe species are well dispersed or framework-incorporated in the zeolite. This aspect was already reported in the literature (Yue et al. 2015). However, it seems more logical that the absence of diffraction lines of Fe₂O₃ in the XRD might be due to the formation of amorphous Fe₂O₃. This certainly occurs because the heat treatment performed during the synthesis was realized at low temperature (100 °C, 24 h).

Diffuse reflectance UV/Visible spectroscopy is employed to characterize the optical properties of the powder materials and also to determine the nature of the iron species in the zeolite structure (Fig. 3b). The spectrum recorded with the non-immobilized Fe₂O₃ particles is also represented in the figure. The raw faujasite displays a strong absorption in the UV-spectral range, between 250 and 350 nm. Conversely, no absorbance can be detected in the visible range between 400 and 800 nm. The spectrum of pure Fe₂O₃ particles appears different. It displays a plateau between 350 and 550 nm, and the absorbance decreases for larger wavelengths. More

Fig. 2 Influence of the iron initial concentration on the atomic percentages and atomic ratios, obtained from EDS emitted by the elements (Fe, Si, and Al) encountered on the surface of bare and modified faujasite



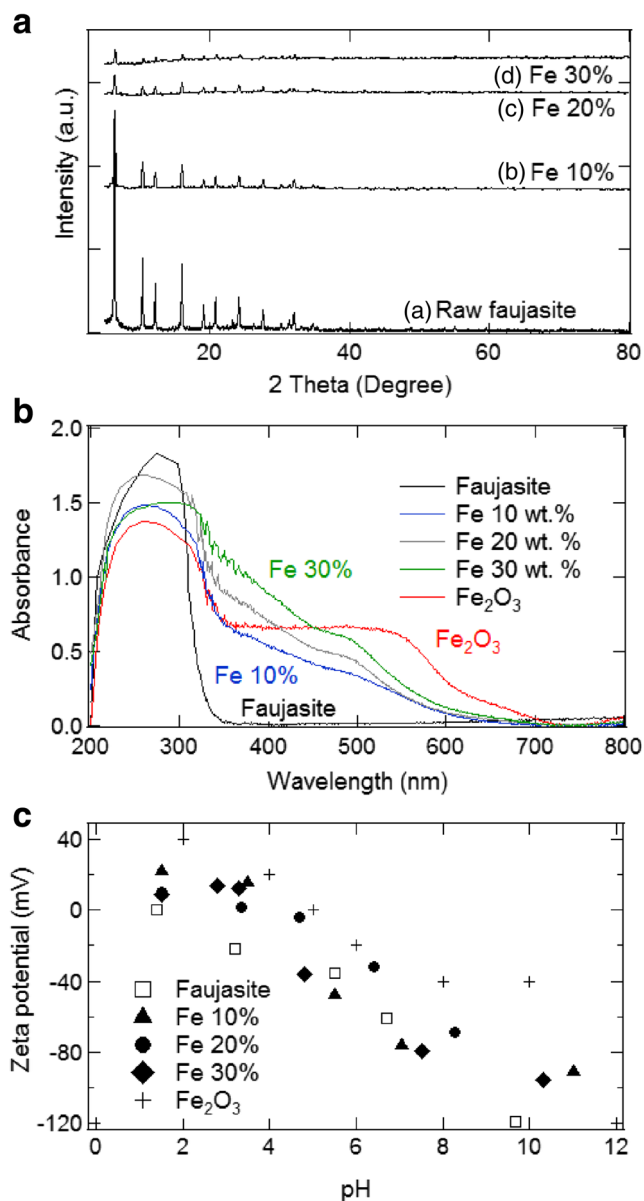


Fig. 3 Characterization of the Fe impregnated faujasite. (A) XRD patterns of Fe impregnated faujasite prepared with initial masses of iron nitrate of: (a) 0%, (b) 10 wt.%, (c) 20 wt.%, and (d) 30 wt.%. (B) Solid absorbance UV/visible spectra for raw faujasite, and zeolite impregnated with various amounts of iron. (C) Zeta potential of bare and iron-covered faujasite samples as a function of the pH

remarkably, in the presence of iron onto the faujasite, the absorbance data seems to be a mix of the spectra of raw faujasite and pure Fe₂O₃. The maximum in absorbance is obtained at a wavelength of 260 nm. This peak corresponds to isolated Fe²⁺ and Fe³⁺ ions (Kowalska-Kuś et al. 2013). In addition, for larger wavelengths, the absorbance decreases continuously up to 600–650 nm. This indicates that the photoresponse of the modified zeolite is successfully extended to the visible region of light. A peak in the UV range 300–400 nm appears for 20 wt.%- and 30 wt.%-impregnated faujasite while it is less intense for 10 wt.%-impregnated form.

This peak corresponds to the small oligonuclear Fe_x³⁺O_y in zeolite channels (Rutkowska et al. 2014). Another peak with a maximum intensity at about 500 nm is observed for the pure Fe₂O₃ particles and the impregnated faujasites. This peak is attributed to the bulky Fe₂O₃ aggregates located on the external surface of the faujasite (Li et al. 2008; Rutkowska et al. 2014). It has a higher intensity for 20 wt.%- and 30 wt.%-impregnated faujasite compared to the 10 wt.%. Additionally, the appearance of this peak for the impregnated faujasite confirms the presence of Fe species, mainly under the form of Fe₂O₃, in the zeolite.

Zeta potential–pH curves are obtained to investigate the surface character of the original zeolite and the iron-coated faujasite (Fig. 3c). The raw faujasite is negative in the whole range of pH. There is a significant increase in the negative charge with the pH. The zeta potential is zero at pH 1–1.5 and it decreases up to pH 10. These values correspond perfectly to the ones mentioned in the literature (Basumatary et al. 2016). The impregnation of iron over faujasite impacts the surface charge behavior. The zeta potential decreases with the pH from positive values in acidic medium (pH < 1.5–4) to negative values at higher pH. The presence of iron onto the zeolite causes a shift of the point of zero charge (PZC) towards larger pH values between 3 and 4. The zeta potential–pH of the composites follows the same trend as compared to that reported for the non-immobilized iron oxide Fe₂O₃ particles but with a shift of the PZC (Andrade et al. 2009; Erdemoğlu and Sarıkaya 2006). The similarity between zeta potential data on the iron-impregnated faujasite and the pure Fe₂O₃ particles suggests that iron oxide particles are deposited onto the surface. An alternative explanation can be also discussed. The impregnation of iron over faujasite hides some Al sites from the surface, thus the PZC shifts to higher pH, and the zeta potential to larger values due to higher acidic strength of the Al atoms (Kuzniatsova et al. 2007).

Photo-Fenton degradation of model pollutant

The photo-Fenton activity of the iron-impregnated zeolite samples has been tested on the photodegradation of phenol. The kinetics of the phenol degradation is analyzed in detail to optimize the performance of both the material and the process. The effect of some physicochemical parameters, such as H₂O₂ concentration, incident light nature and intensity, amount of iron deposited onto the faujasite, and pH, has been varied. Prior to analysis of the degradation results, it seems interesting to discuss the adsorption capability of the modified zeolites (results not shown). A very weak adsorption of phenol onto bare and Fe-impregnated faujasite is obtained. The pollutant uptake does not significantly vary with the iron surface concentration. This low adsorption is mainly due to the hydrophilic nature of phenol bearing a hydroxyl OH group that makes its interaction with the hydrophobic zeolite negligible.

The presence of hydrogen peroxide is an important parameter required for the degradation of the pollutants in heterogeneous photo-Fenton process. The dependence of the hydrogen peroxide concentration on the time course of the UV photo-Fenton degradation of phenol is illustrated in Fig. 4a. Each curve shows the bulk concentration of phenol as a function of the time of treatment. In the absence of hydrogen peroxide, no diminution of the phenol concentration with the process time can be detected. This validates the lack of degradation in the absence of H₂O₂, and also the fact that the UV photolysis of phenol is negligible. Conversely, in the presence of H₂O₂, the bulk concentration of phenol declines over photo-Fenton process time. The total degradation is obtained using the four different concentrations of hydrogen peroxide. The degradation becomes faster as the concentration of hydrogen peroxide increases up to 0.015 M. Then, H₂O₂ concentrations of 0.015 M and 0.06 M give very similar removal efficiency. The presence of hydrogen peroxide allows the production of hydroxyl radicals through the mechanisms given in Eqs. (1)–(9) (Ghaly et al. 2001). At low concentration of hydrogen peroxide, the production of hydroxyl radicals remains low, thus, resulting in slow oxidation rate. When the concentration of H₂O₂ becomes higher, the amount of hydroxyl radicals

used for phenol oxidation increases (Kasiri et al. 2008). This enhances the probability of reaction between the pollutant molecules and the oxidizing species leading to a rise of the degradation rate. However, there is an optimum in the H₂O₂ concentration, i.e., 0.015 M, since larger hydrogen peroxide concentrations do not lead to higher removal rate. Actually, as soon as all the Fe²⁺ and Fe³⁺ have reacted with the H₂O₂, whatever the hydrogen peroxide content remaining in the solution, they will not be able to produce supplementary hydroxyl radicals by the Fenton reaction (Eqs. (1)–(6)).

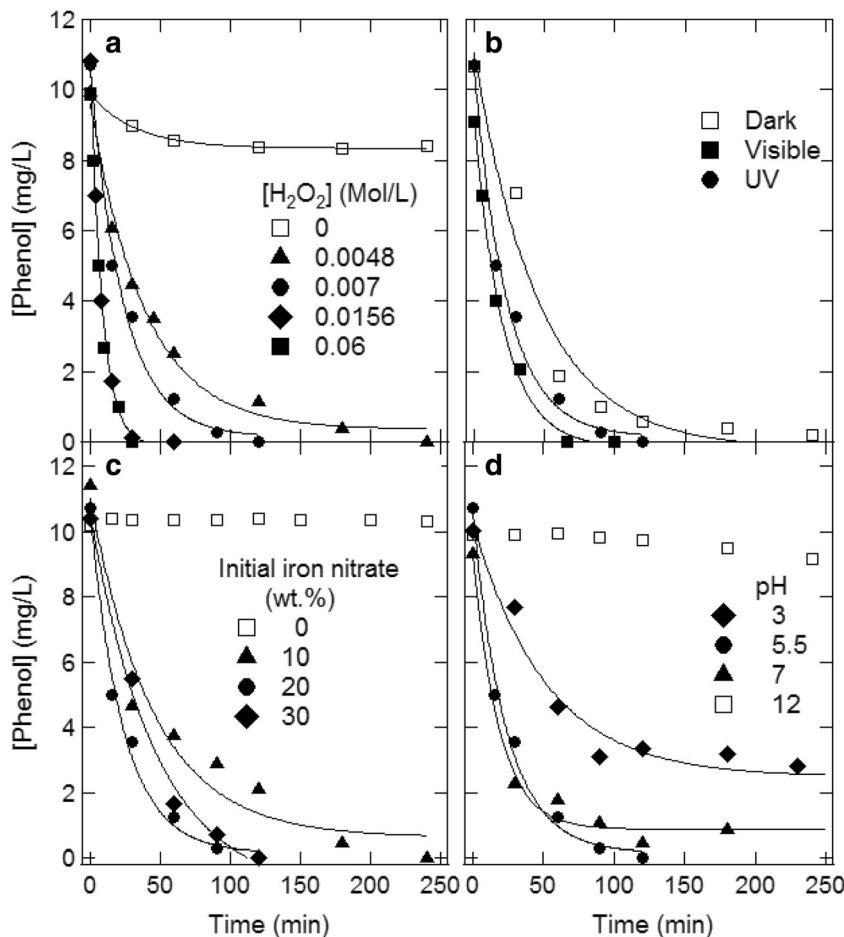
The variation of the phenol concentration (C) with respect to the time of the process (t) corresponds to an exponential decay shape, which is characteristic of a first-order kinetic reaction regardless of the hydrogen peroxide content:

$$C = C_0 \exp(-k t) \tag{10}$$

Note that C₀ stands for the initial pollutant concentration in the bulk solution at the beginning of the photo-Fenton process. Table S4 of the Supporting information illustrates the effect of the H₂O₂ content on the values of the reaction rate constant k.

The phenol mineralization is examined by TOC analysis at the end of the photo-Fenton process, i.e., when the phenol concentration becomes equal to zero (Table S4 of the

Fig. 4 Optimization of the experimental parameters during the photo-Fenton degradation of phenol using Fe impregnated faujasites. **(a)** Effect of the concentration of H₂O₂. Experimental conditions: catalyst concentration = 1 g/L, UV light, and pH 5.5. **(b)** Influence of the light nature. Experimental conditions: catalyst concentration = 1 g/L, 0.007 M H₂O₂, and pH 5.5. **(c)** Effect of the initial masses of iron nitrate nonahydrate used to prepare the iron/faujasite composites. Experimental conditions: catalyst concentration = 1 g/L, 0.007 M H₂O₂, UV light and pH 5.5. **(d)** Influence of pH. Experimental conditions: catalyst concentration = 1 g/L, 0.007 M H₂O₂, and UV light. The lines correspond to the fit of the experimental data by a first-order exponential decay function of the form $A \exp(-k t)$ consistent with a first-order kinetics



Supporting information). In the presence of H_2O_2 , the TOC value increases with the concentration of H_2O_2 . A weak carbon content remains in solution ($[\text{TOC}] = 1.7\text{--}2.1 \text{ mg C/L}$) for H_2O_2 concentrations of 0.007 and 0.0048 M. It seems now established that a TOC value lower than or equal to 2.5 mg C/L indicates the quasi-complete mineralization of the pollutant. No organic by-product is produced during the degradation, and the quasi-complete mineralization of phenol takes place for H_2O_2 concentrations of 0.007 and 0.0048 M. To investigate the most efficient H_2O_2 content to be used, the rate constants of phenol degradation of the different tests are compared to the H_2O_2 concentration. The system with the highest rate constant and the lowest H_2O_2 concentration used is the most efficient. For this reason, the ratios of the rate constant are normalized by the concentration of H_2O_2 , i.e., the $[\text{H}_2\text{O}_2]/k$ ratios are calculated. The calculated ratios for the tests with H_2O_2 concentrations of 0.0048, 0.007, 0.0156, and 0.06 M are equal to 0.192, 0.179, 0.106, and 0.444 mol min/L, respectively. As seen from the ratios obtained, H_2O_2 concentrations of 0.007 and 0.0156 M lead to the lowest ratio with close values. Based on all these data, a concentration of hydrogen peroxide of 0.007 M was chosen to be used in all the experiments.

Incident light nature and intensity can affect the degradation efficiency of the iron-impregnated faujasite. Series of experiments are carried out in the absence of illumination (“Dark”), under UV and visible irradiations (Fig. 4b). The complete phenol degradation is achieved in the absence of illumination, under UV and visible light irradiation. The TOC analysis is employed to support this interpretation. The TOC values of the solutions at the end of the degradation process range between 1.9 and 2.1 mg C/L (Table S5 of the Supporting information) confirming the quasi-complete mineralization of the contaminants and also the absence of by-products. However, the nature and the intensity of the light affect the kinetics of degradation. The phenol solutions become fully degraded within 60 min under visible light, 90 min under UV light, and 240 min in the absence of light. Faster degradation occurs under irradiation. The presence of UV radiations enhances the photolysis of hydrogen peroxide and thus the amount of hydroxyl radicals produced (Eq. (9)). Another consequence could be the photo-reduction of Fe(III) to Fe(II) ions, in the presence of illumination. The produced Fe(II) can react with hydrogen peroxide molecules and leads to the production of additional hydroxyl radicals through Fenton reaction, i.e. Eqs. (7) and (8) (Kasiri et al. 2008).

To compare the efficiency of both UV and visible light, the rate constants for the catalytic tests under both light illumination are calculated. The fit of the experimental data by a first-order exponential decay function of the form $A \exp(-k t)$ confirms a first-order degradation mechanism independently of the light nature. The deduced rate constants k are reported in

Table S5 of the Supporting information. Recall that the size of the reactor is affected by the type of illumination source, i.e., for the experiments under UV light, volume of solution up to 200 mL can be used, while the volume remains limited to 40 mL when performing degradation under visible light because of the optical fiber. For this reason, the volume of the reaction mixture treated has to be taken into consideration. This is done by normalizing the rate constants (k) by the volume (V) of the reaction mixture used, i.e., the test with higher rate constant and larger volume of reaction mixture treated shows better efficiency. Under UV light, $k \times V$ factor is 3.152 mL/min which is greater than under visible light where $k \times V = 2 \text{ mL/min}$. Therefore, the following experiments will be carried out under UV light illumination.

The effect of the iron content immobilized onto the zeolite on the kinetics of the UV photo-Fenton degradation of phenol is illustrated in Fig. 4c. In the absence of iron deposited onto the faujasite, no change in the concentration of phenol during the treatment can be detected. So, we can conclude that the faujasite alone does not have any degradation effect on phenol. In the presence of iron onto the faujasite, an increase of the degradation rate with the initial mass of iron nitrate nonahydrate from 10 wt.% to 20 wt.% is observed. The kinetic constant k increases from 0.016 to 0.039 min^{-1} (Table S6 of the Supporting information). Another interesting feature is that the degradation rate reaches a constant value at iron concentrations larger than or equal to 20 wt.% ($k = 0.03\text{--}0.039 \text{ min}^{-1}$). It appears more suitable to discuss the relationship between the degradation rate and the real iron amount deposited onto the zeolite, derived from the EDS data (Fig. 2). A substantial enhancement in the amount of Fe deposited onto the faujasite surface between 10 wt.% (Fe = 5.56 wt.%) and 20 wt.% (Fe = 12.89 wt.%) is demonstrated. The increase in the degradation rate is mainly due to the greater loading of iron onto the zeolite surface that is involved in the photo-Fenton heterogeneous process, thus, improving the quantity of hydroxyl radicals. At higher iron dose, i.e., when the initial concentration of iron in solution increases beyond 20 wt.%, the deposited uptakes remain constant and equal to ca. 12–13%. In this range of iron content, no difference in the temporal evolution of the phenol degradation can be observed. In order to analyze the data more deeply, the TOC and Fe concentrations at the end of the heterogeneous photo-Fenton process are given in Table S6 of the Supporting information. The TOC decreases with the amount of iron deposited from 2.3 to 1.0 mg C/L. These low carbon contents confirm the quasi-complete mineralization of the phenol regardless of the iron loading deposited onto the zeolite. At the same time, the iron concentration in solution increases, from 0.7 to 4.4 mg/L, with the amount of iron immobilized. The sample containing theoretically

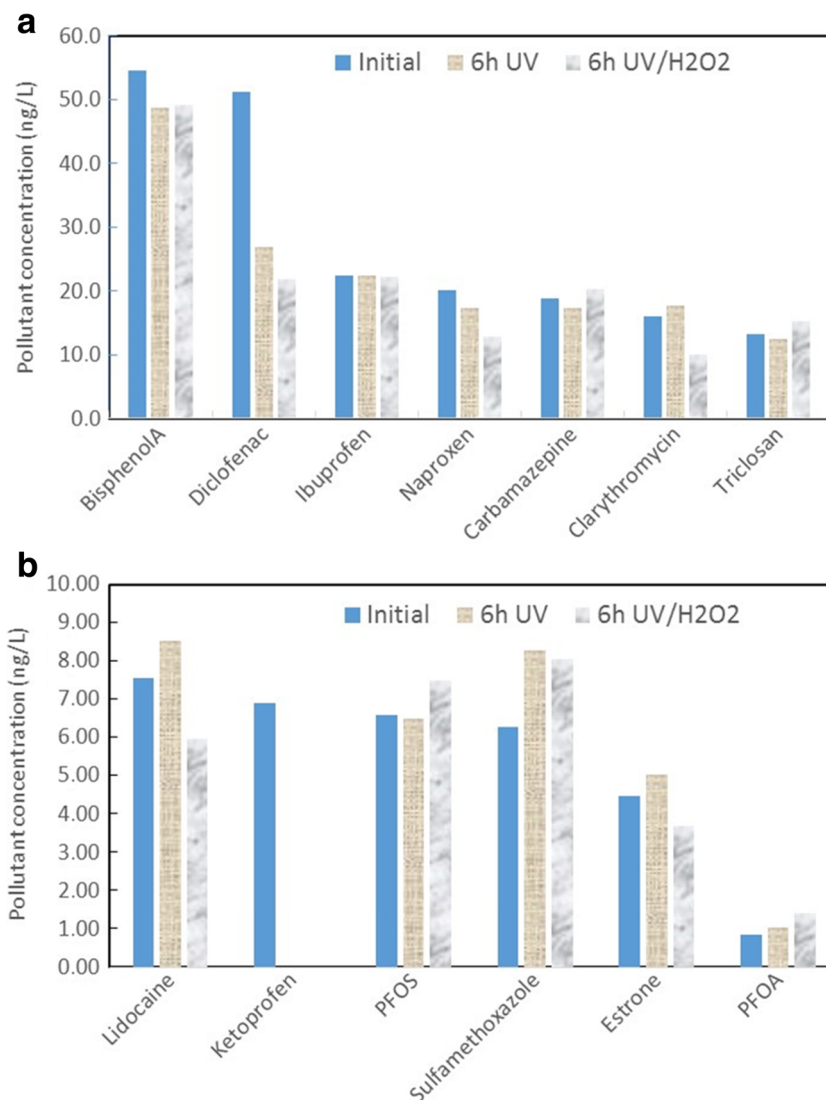
20 wt.% of iron seems sufficient to reach quickly a total phenol degradation while maintaining a fair amount of lixiviated iron. Consequently, this sample has been selected for the next experiments.

The effect of the pH on the photo-Fenton degradation of phenol is examined in amplitude pH of 3–12 in the presence of 20 wt.% Fe-impregnated faujasite catalyst. The results are depicted in Fig. 4d and Table S7 of the Supporting information. The maximum degradation efficiency is obtained at pH 5.5 (natural pH of the phenol solution) and pH 7. The pH value 5.5 is generally considered as the optimum pH in heterogeneous Fenton process using Fe-zeolite systems in the literature (Kasiri et al. 2008; Neamu et al. 2004a). We notice also a lower degradation efficiency at pH 3 and a lack of degradation activity at pH 12. The optimum activity of the catalyst at pH 5.5 is related to the nature of the environment of the iron cations inside the pore structure of the zeolite even

though the distribution of the iron species in this environment has not been elucidated yet. A strong electrostatic interaction is present between the positively charged Fe cations and the negatively charged zeolite framework. This interaction can prevent or slow down the precipitation of iron hydroxides even at quasi-neutral pH values (Neamu et al. 2004b). Moreover, other parameters can explain the change of the catalyst activity with pH. On the one hand, the pH of the solution is regulated from pH 5.5 to pH 3 using hydrochloric acid. Consequently, a high amount of Cl⁻ ions was added to the phenol solution. The chloride ions have the ability to deactivate the hydroxyl radicals (Eq. (11)). This causes a decline in the degradation efficiency since the formed inorganic radical anions present a very low reactivity compared to that of [•]OH (Kasiri et al. 2008).



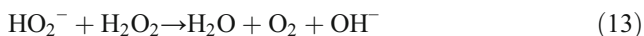
Fig. 5 Blank experiments in the absence of the iron-impregnated faujasite under UV illumination (“6 h UV”) or in the simultaneous presence of UV and H₂O₂ (6 h UV/H₂O₂). The notation “Initial” indicates the initial micropollutant concentration before the treatment



On the other hand, at very basic pH (pH 12), the hydrogen peroxide decomposition becomes favored, increasing the amount of conjugate base HO_2^- in the solution (Eq. (12)).



The formed conjugate base (HO_2^-) produces a double scavenging effect. First, it can react with the H_2O_2 molecules (Eq. (13)) restricting the production of hydroxyl radicals. Second, it can also deactivate the hydroxyl radicals (Eq. (14)).



The formed oxygen anion radical has a very low reactivity with organic pollutants in comparison with that of H_2O_2 and $\cdot\text{OH}$ (Li et al. 2006).

For an optimal choice of the pH, it seems also relevant to discuss the remaining TOC and the lixiviated iron at the end of the heterogeneous photo-Fenton process (Table S7 of the Supporting information). The minimum TOC content (2.1 mg C/L) and iron concentration (3.9 mg/L) are obtained at the natural pH of the phenol solution, i.e., pH 5.5. Consequently, the pH will be set at 5.5 for all the experiments with real water.

Photo-Fenton degradation of micropollutants from real water

The photo-Fenton process is used with real water samples from the Meurthe river. The faujasite containing 20 wt.% of iron was used as catalyst. All the results are listed in Table S8 of the Supporting information.

Fig. 6 Adsorption of the micropollutants onto the iron-impregnated faujasite. The notation “Initial” indicates the initial micropollutant concentration before the treatment, while “2 h dark” corresponds to the micropollutants concentration remaining in solution after 2 h of contact between the water and the catalyst in the dark and in the absence of H_2O_2 . The specific legend “under limit” indicates that the concentration remains lower than the limit of quantification of the LC-MS/MS. The dotted lines give also the limit of quantification of the LC-MS/MS. Experimental conditions: catalyst concentration = 1 g/L, and pH 5.5

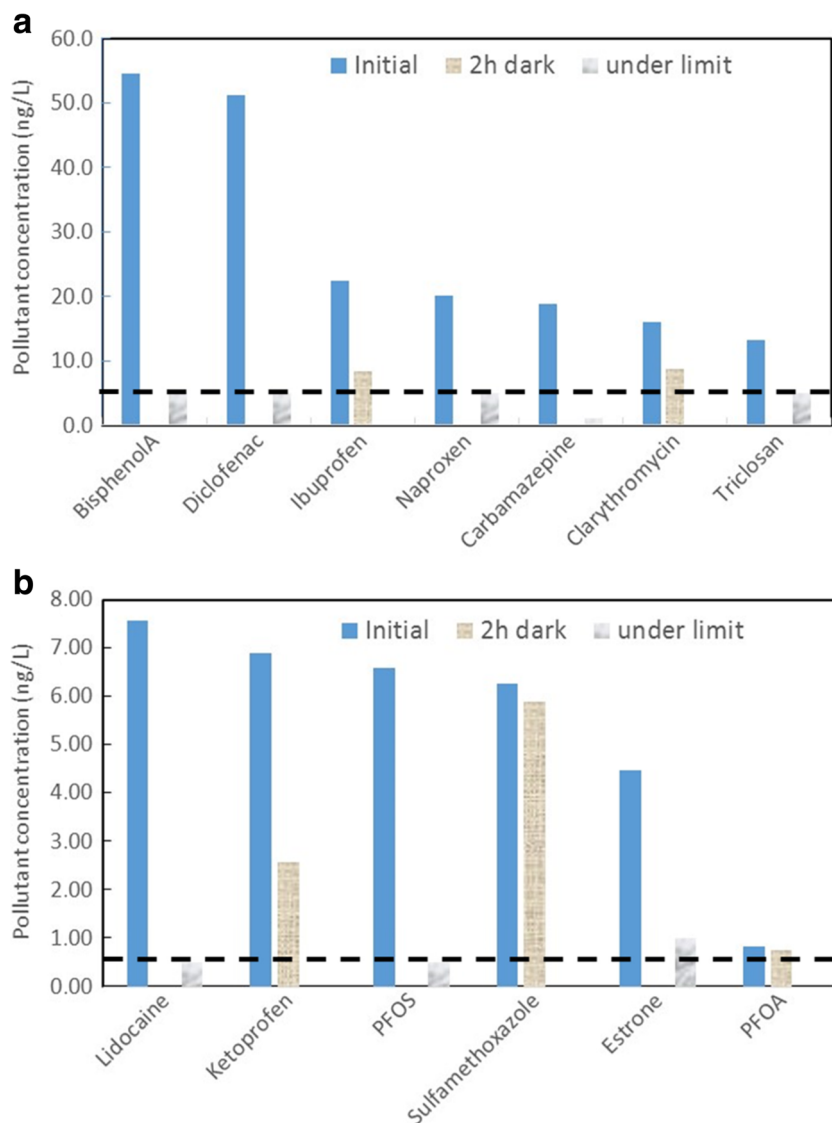
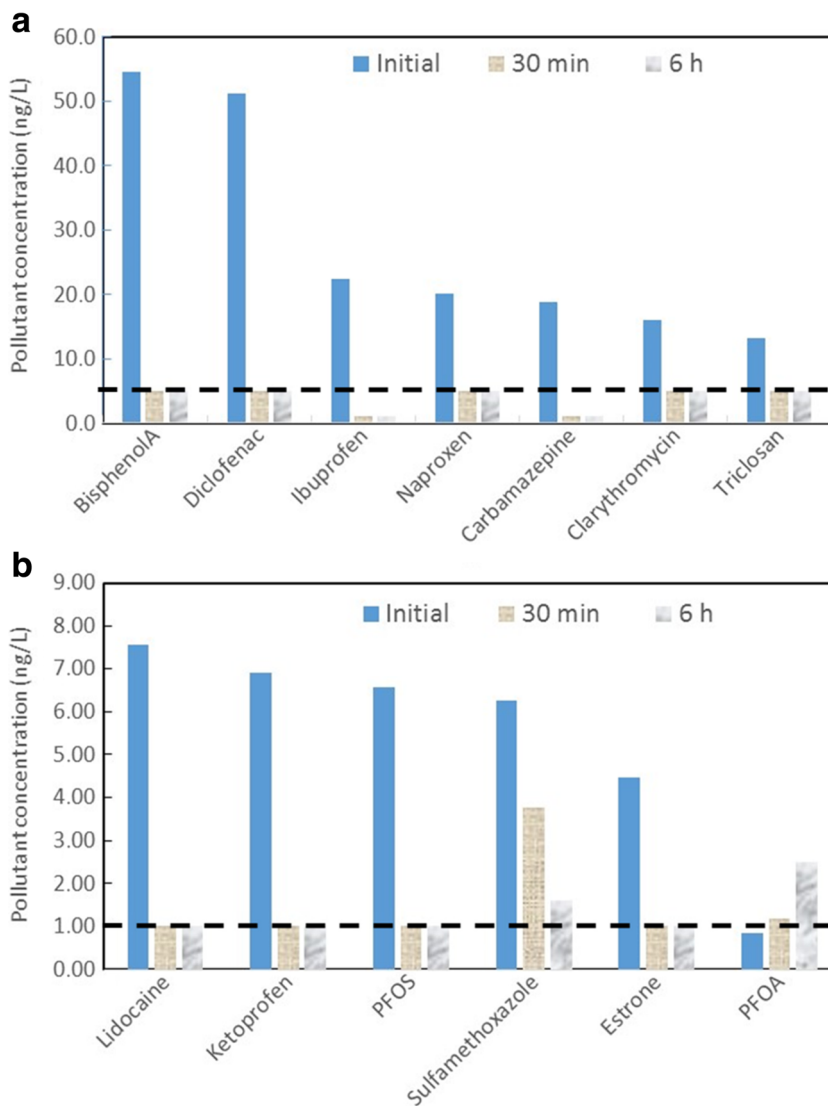


Fig. 7 Photo-Fenton treatment of the water using iron-impregnated faujasite. The notation “Initial” indicates the initial micropollutant concentration before the treatment, while “30 min” and “6 h” correspond to the micropollutant concentrations remaining in the solution after 30 min and 6 h of photo-Fenton process. The dotted lines give the limit of quantification of the LC-MS/MS. Experimental conditions: catalyst concentration = 1 g/L, 0.007 M H₂O₂, UV light and pH 5.5



First, it is interesting to analyze the initial concentration of the micropollutants before the water treatment process (Fig. 5). All the concentrations remain in the range of nanogram per liter. The maximum concentration measured is equal to approximately 50 ng/L. It is recorded for diclofenac and bisphenol A. On the one hand, the presence of carbamazepine-10,11-epoxide, cyclophosphamide, erythromycin, estradiol-beta, ethynylestradiol, sulfadimethoxine, sulfadimidine, and sulfathiazole is detected. However, their concentrations fall under the limit of quantification of the LC-MS/MS apparatus. On the other hand, the micropollutant initial concentrations decrease from 54 to 1 ng/L in the following order: bisphenol A (54 ng/L), diclofenac (51 ng/L), ibuprofen (22 ng/L), naproxen (20 ng/L), carbamazepine (19 ng/L), clarithromycin (16 ng/L), triclosan (13 ng/L), lidocaine (7 ng/L), ketoprofen (7 ng/L), PFOS (6 ng/L), sulfamethoxazole (6 ng/L), estrone (4 ng/L), and PFOA (0.8 ng/L).

It appears also necessary to perform blank experiments in the absence of the iron-impregnated faujasite under UV illumination and in the presence of H₂O₂ (Fig. 5). For the majority of the micropollutants, the photolysis of the contaminants can be neglected since the pollutant concentrations do not vary after 6 h under UV irradiation. At the same time, the degradation remains also negligible in the presence of hydrogen peroxide. However, the concentration of ketoprofen after 6 h of UV becomes lower than the quantification limit of the analytical system regardless of the presence of H₂O₂. For this reason, this pollutant cannot be considered in the photo-Fenton analysis. It is also important to note that the photolysis and the effect of hydrogen peroxide cannot be neglected with diclofenac. The contaminant concentration drops from 51 to 27–22 ng/L after 6 h of irradiation. In addition, a weak degradation occurs for bisphenol A (from 54 to 49 ng/L),

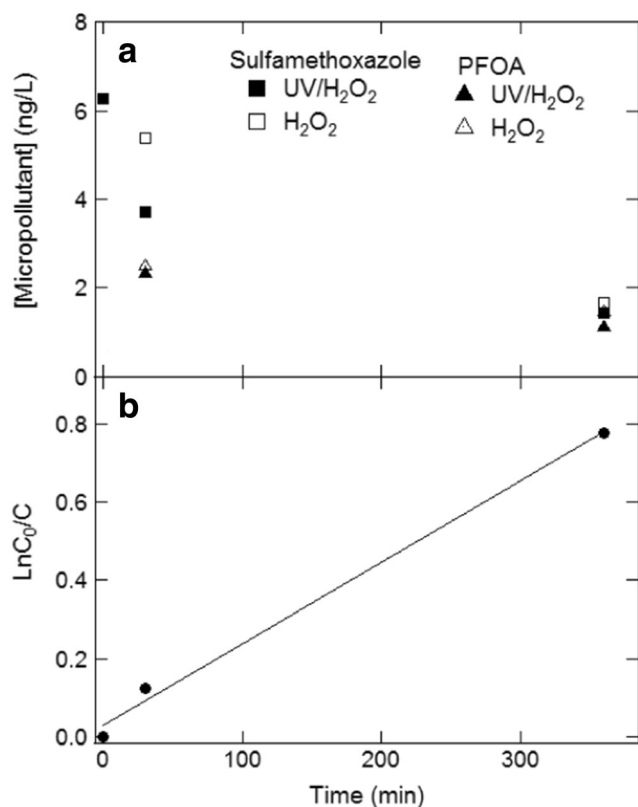


Fig. 8 (a) Effect of the illumination on the degradation performances. The photo-Fenton data (“UV/H₂O₂”) are compared to the Fenton results in the dark (“H₂O₂”) for sulfamethoxazole and PFOA micropollutants. (b) Kinetics of sulfamethoxazole photo-Fenton degradation by the iron-impregnated faujasite (20 wt.% Fe). Linear transform: $\ln(C_0/C)$ versus time. The line represents the best linear fit given by $\ln(C_0/C) = 0.0021 \text{ time} + 0.029$ ($R^2 = 0.9947$). Experimental conditions: catalyst concentration = 1 g/L, 0.007 M H₂O₂, and pH 5.5

naproxen (from 20 to 17–13 ng/L), and clarithromycin (from 16 to 10 ng/L).

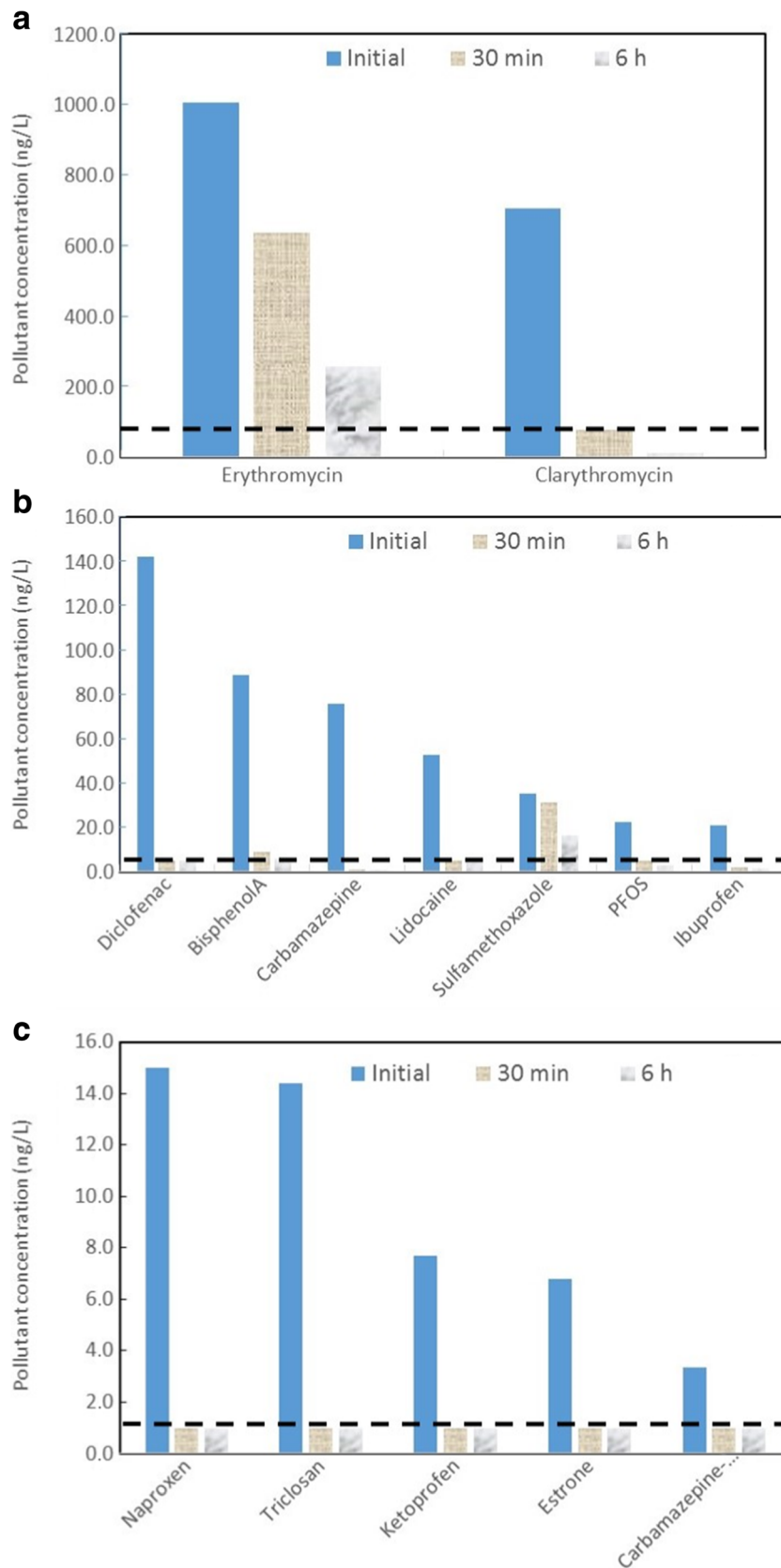
The main part of the decomposition processes is expected to take place onto the surface of the catalyst. Consequently, the adsorption features could be one of the factors that drives the photo-Fenton performance. To explore in detail the adsorption of the micropollutants onto the iron-impregnated faujasite, the contaminant concentrations are analyzed after 2 h of contact between the water and the catalyst (Fig. 6). The data correspond to the remaining pollutant concentration after 2 h of stirring in the dark and in the absence of H₂O₂. Consequently, they give access to the adsorption capability of the samples. For bisphenol A, diclofenac, naproxen, carbamazepine, triclosan, lidocaine, PFOS, and estrone, the concentrations after 2 h in the dark appear below the limit of quantification of the LC-MS/MS system. This indicates a large and substantial adsorption of these contaminants onto the Fe/faujasite. For instance, in the presence of all the other micropollutants, the adsorption of the diclofenac from an initial solution of 50 ng/L appears significant due to the high

affinity of this pollutant for the faujasite surface. These results emphasize also that all these micropollutants can be efficiently removed from the water by the adsorption process. Oppositely, for ibuprofen, clarithromycin, and ketoprofen, a non-negligible adsorption takes place after 2 h of contact with the modified faujasite in the dark. However, some of these micropollutants remain in the water. At the same time, the absence of adsorption of sulfamethoxazole and PFOA onto the iron-impregnated zeolite has to be mentioned.

We move now to the case of the photo-Fenton treatment of the water (Fig. 7). Except for sulfamethoxazole and PFOA, the concentration of all the other micro-contaminants becomes lower than the limit of quantification of the LC-MS/MS after 30 min of photo-Fenton treatment. This does not necessarily demonstrate a total degradation of the pollutants, but this emphasizes that, at least, a very low concentration of these micropollutants remains in the solution. This indicates the good efficiency of the photo-Fenton process using iron-impregnated faujasite with a cocktail of a minimum of 21 micropollutants. We can also stress the quicker degradation with the mixture of the micropollutants (30 min) compared to the time necessary to degrade a larger concentration of phenol (10 mg/L), which takes 100 min. However, the comparison of the initial TOC values of the solutions, i.e., 2.8 mg C/L for the water containing the micropollutants and 6.8 mg C/L for the phenol solution, demonstrates that a greater amount of phenol macro-pollutant has to be degraded in comparison to the sum of all the micropollutants present inside the real water. However, the complete degradation of sulfamethoxazole does not occur. The initial concentration of 6.2 ng/L decreases to 3.7 ng/L after 30 min of process, and then to 1.6 ng/L after 6 h of photo-Fenton treatment. This indicates that the kinetic of degradation is slower than for the other micropollutants. In addition, the degradation of PFOA can be neglected since the micropollutant concentration does not vary after 6 h of the process.

It appears relevant to address the effect of the illumination on the degradation performances. In that respect, the photo-Fenton data (“UV/H₂O₂”) are compared to the Fenton results in the dark (“H₂O₂”) in Fig. 8a. As previously reported during the degradation of the model phenol macro-pollutant, a weak effect of the UV irradiation is observed. A slight improvement of the degradation efficiency of the micropollutants occurs in the presence of UV in comparison to that reported in the dark. For instance, the

Fig. 9 Photo-Fenton treatment of the water using iron-impregnated faujasite. The sampling was performed in November 2016. The notation “Initial” indicates the initial micropollutant concentration before the treatment, while “30 min” and “6 h” correspond to the micropollutant concentrations remaining in the solution after 30 min and 6 h of photo-Fenton process. The dotted lines give the limit of quantification of the LC-MS/MS. Experimental conditions: catalyst concentration = 1 g/L, 0.007 M H₂O₂, UV light and pH 5.5



concentration of sulfamethoxazole after 30 min of treatment becomes equal to 5.3 ng/L in the absence of illumination (Fenton)

while it drops to 3.7 ng/L under UV illumination (photo-Fenton). The same trend is reported for PFOA. Nevertheless, it is

interesting to note that for all the other micropollutants, 30 min of Fenton process in the dark is sufficient to reach concentrations below the limit of quantification of the analytical apparatus (Table S8 of the Supporting information). The same behavior was also observed in the presence of UV illumination.

Finally, to test the effect of the micropollutant concentration, additional data corresponding to photo-Fenton experiments performed with new water are discussed (Fig. 9 and Table S9 of the Supporting information). The water was sampled from the same location in the Meurthe river but at a different period. The sampling was performed in November 2016 while it was carried out in March 2017 for the previous experiments. The initial concentration of the micropollutants is higher inside the water taken in November. This allows us to evaluate the efficiency of the photo-Fenton process in the presence of a larger contaminant content. Consequently, the degradation of new molecules such as carbamazepine-10,11-epoxide and erythromycin can be tested since their initial concentrations become larger than the limit of quantification of the LC-MS/MS. After 30 min of photo-Fenton treatment, the total abatement of lidocaine, naproxen, triclosan, carbamazepine, carbamazepine-10,11-epoxide, diclofenac, and estrone occurs. These results corroborate our previous measurements obtained during the first sampling (March 2017) despite the larger micropollutant concentrations. After 6 h of photo-Fenton process, clarithromycin disappears. In addition, bisphenol A, erythromycin, ibuprofen, and PFOS are not completely removed after 6 h of treatment but their initial concentrations have been reduced by a factor larger than or equal to 10.

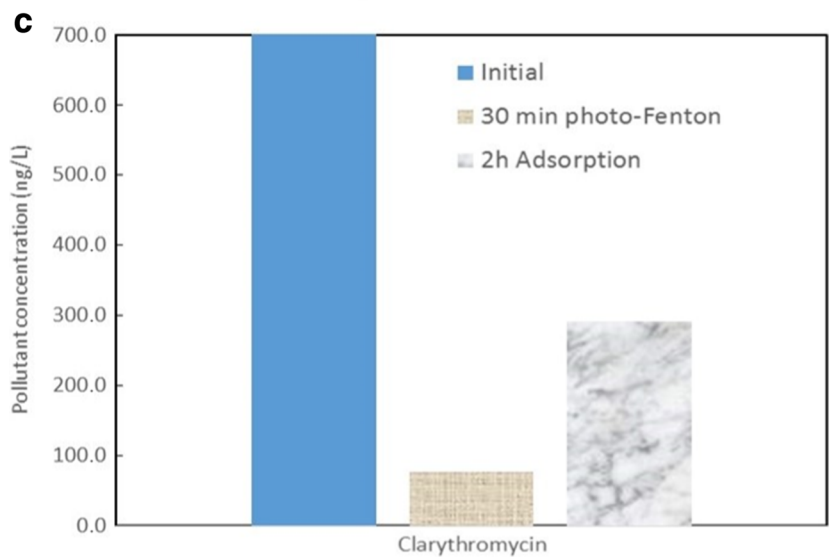
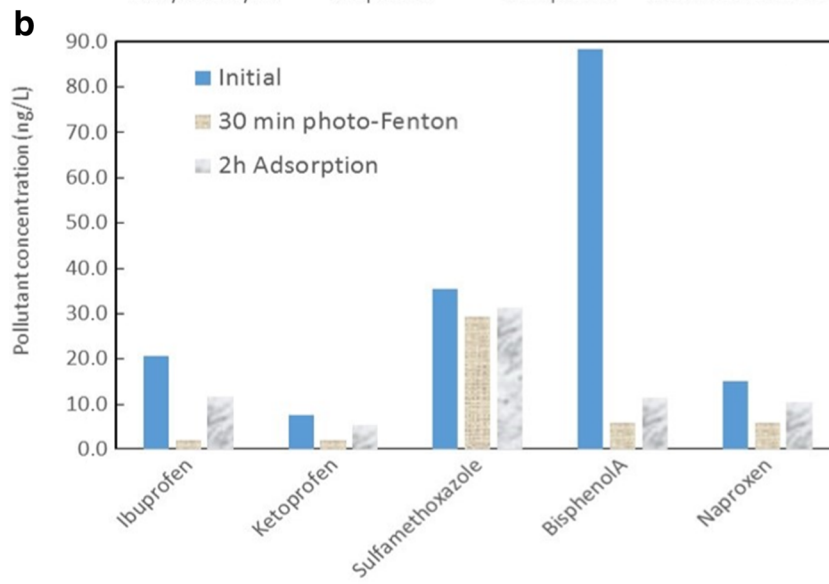
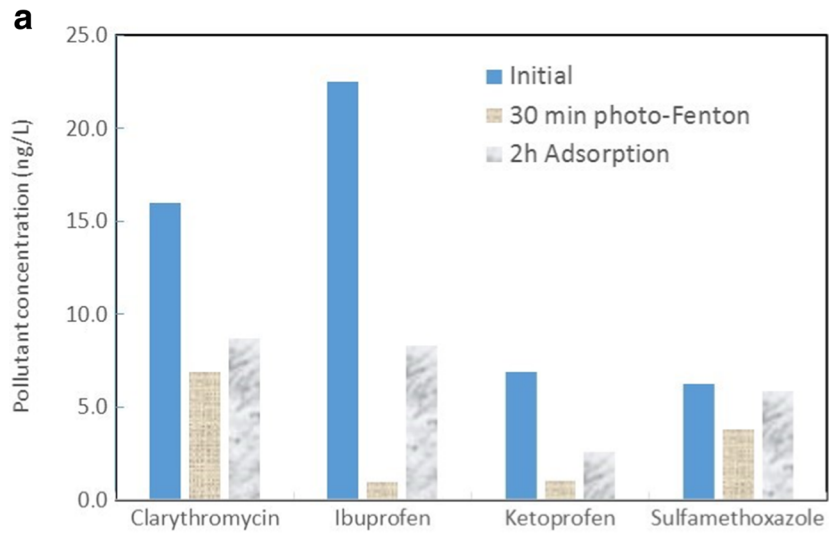
For ibuprofen, ketoprofen, and triclosan, the initial concentrations are similar between the two samplings. These data can be analyzed in order to have an idea of the reproducibility of the measurements and the degradation process. In both cases, the photo-Fenton treatment leads to the disappearance of triclosan after 30 min. The adsorbed amount of ketoprofen onto the Fe/faujasite remains very close. In the special case of ibuprofen, the kinetic of degradation does not quantitatively differ from the first result and the trends are similar.

Using the new data obtained at larger initial concentrations, it becomes possible to examine the kinetics of the photo-Fenton degradation for some micropollutants. Particularly, the temporal evolution of the concentration of sulfamethoxazole gives a lot of relevant information. Based on our previous experiments with phenol (macro-pollutant, 10 mg/L), the photo-Fenton degradation is expected to follow a first-order kinetics with respect to the sulfamethoxazole concentration in the bulk solution (C). A plot of $\ln(C_0/C)$ versus the time is shown in Fig. 8b. Note that C_0 stands for the initial micropollutant concentration in the bulk solution (at time = 0). The linear increase of $\ln(C_0/C)$ as a function of time confirms that the photo-Fenton degradation of sulfamethoxazole obeys first-order kinetics in the presence of the cocktail of the

other micropollutants. The linearization gives a kinetic constant k of 0.0021 min^{-1} . We stress that great care has to be taken with the value of this constant because it was obtained with only three experimental data, which do not ensure a great accuracy. However, the k value can be compared with the kinetic constant already obtained with phenol. We found a constant of 0.0394 min^{-1} for the photo-Fenton degradation of an initial solution containing 10 mg/L of phenol. The lower value obtained with the sulfamethoxazole from the real water can be explained by the competition between all the micropollutants for the iron catalysts active sites of the faujasite surface.

It seems also interesting to discuss the relative importance of the photo-Fenton and the adsorption effects to remove the micropollutants from the real water using iron-impregnated faujasite. For this purpose, the remaining microcontaminant concentrations are analyzed after 2 h of adsorption and after 30 min of photo-Fenton treatment. For carbamazepine, carbamazepine-10,11-epoxide, triclosan, estrone and lidocaine, the two concentrations are similar and lower than the limit of quantification of the LC-MS/MS. For these contaminants, it is impossible to discriminate between the effect of the adsorption and the photo-Fenton degradation. In other words, it is not possible to conclude that the micropollutant concentrations decrease due to adsorption or/and photo-Fenton effect with radical production. It appears more relevant to address the other micropollutants for which the concentrations after the adsorption process and the photo-Fenton treatment are different. The results are depicted in Fig. 10 for the waters sampled in March 2017 (Fig. 10a) and November 2016 (Fig. 10b,c). For clarithromycin, ibuprofen, ketoprofen, sulfamethoxazole, bisphenol A, and naproxen, the microcontaminant concentrations after 30 min of photo-Fenton are lower than those after 2 h of adsorption. Consequently, the photo-Fenton treatment shows superior degradation efficiency than the adsorption process. These results confirm that photo-Fenton degradation could be one of the main causes of the high activity during the removal of these micropollutants using iron-impregnated faujasite. This is not surprising since the heterogeneous photo-Fenton process can be viewed as the sum of the adsorption and radical generation. In other words, the high contaminant surface concentration provides a large amount of molecules to react with the hydroxyl radicals generated by light and iron.

Fig. 10 Comparison between the photo-Fenton and the adsorption effect to remove the micropollutants from the real water using iron-impregnated faujasite. The sampling was performed in (a) March 2017 and (b,c) November 2016. The notation “Initial” indicates the initial micropollutant concentration before the treatment, while “30 min photo-Fenton” corresponds to the micropollutant concentration remaining in the solution after 30 min of photo-Fenton process. The notation “2 h Adsorption” represents the micropollutant concentration remaining in solution after 2 h of contact between the water and the catalyst in the dark and in the absence of H_2O_2



Conclusions

The aim of this paper was to evaluate, for the first time, the heterogeneous photo-Fenton degradation of some micropollutants inside real water samples from a river using faujasite Y zeolite impregnated with iron. The catalyst was prepared by the wet impregnation method using iron (III) nitrate nonahydrate as iron precursor. The characterization methods, such as SEM coupled with EDS, XRD, diffuse reflectance UV/visible spectroscopy, and zeta potential, confirm the presence of Fe species, mainly under the form of Fe_2O_3 , deposited onto the surface of the zeolite. The photo-Fenton activity of the iron-impregnated faujasite samples has been optimized on the removal of 10 mg/L of phenol employed as model macro-pollutant. Complete photo-Fenton degradation of the contaminant was achieved using faujasite containing 20 wt.% of iron, under UV light, and in the presence of 0.007 mol/L of H_2O_2 at pH 5.5.

In a second step, the process was used with real water samples from the Meurthe river. Two samplings were carried out in November 2016 and in March 2017. Twenty-one micropollutants including 17 pharmaceutical compounds were specifically targeted, detected, quantified, and degraded. All the initial concentrations remained in the range of nanogram per liter (0.8–88 ng/L). The majority of the micropollutants possessed a large affinity for the surface of the iron-impregnated faujasite. The results demonstrated the good efficiency of the photo-Fenton process with the cocktail of 21 micropollutants. Except for sulfamethoxazole and PFOA, the concentrations of all the other microcontaminants (bisphenol A, carbamazepine, carbamazepine-10,11-epoxide, clarithromycin, diclofenac, estrone, ibuprofen, ketoprofen, lidocaine, naproxen, PFOS, triclosan, etc.) became lower than the limit of quantification of the LC-MS/MS after 30 min or 6 h of photo-Fenton treatment depending on their initial concentrations. In the presence of the cocktail of the other micropollutants, the photo-Fenton degradation of PFOA can be neglected, while the degradation of sulfamethoxazole obeys first-order kinetics.

The photo-Fenton degradation performances of the iron impregnated faujasite towards the cocktails of micropollutants are promising. The removal of micropollutants at such low concentration is representative of the emerging contaminant concentration level (ng/L) encountered at the outlet of the WWTP. Consequently, the results can be directly applied at the level of industrial scale in wastewater treatment plants. Future work will extend the present work to address more specifically the degradation mechanisms (byproducts) and also chemical engineering aspects, such as reactor design, in order to evaluate the potential scale-up of this process to real wastewater treatment plants.

References

- Andrade AL, Souza DM, Pereira MC, Fabris JD, Domingues RZ (2009) Synthesis and characterization of magnetic nanoparticles coated with silica through a sol-gel approach. *Cerâmica* 55(336):420–424. <https://doi.org/10.1590/S0366-69132009000400013>
- Arimi M (2017) Modified natural zeolite as heterogeneous Fenton catalyst in treatment of recalcitrants in industrial effluent. *Progress Nat Sci: Mater Int* 27(2):275–282. <https://doi.org/10.1016/j.pnsc.2017.02.001>
- Arvaniti O, Stasinakis A (2015) Review on the occurrence, fate and removal of perfluorinated compounds during wastewater treatment. *Sci Total Environ* 524–525:81–92. <https://doi.org/10.1016/j.scitotenv.2015.04.023>
- Barakat MA, Tseng JM, Huang CP (2005) Hydrogen peroxide-assisted photocatalytic oxidation of phenolic compounds. *Appl Catal B* 59(1):99–104
- Barreca S, Velez Colmenares J, Pace A, Orecchio S, Pulgarin C (2014) Neutral solar photo-Fenton degradation of 4-nitrophenol on iron-enriched hybrid montmorillonite-alginate beads (Fe-MABs). *J Photochem Photobiol A* 282:33–40. <https://doi.org/10.1016/j.jphotochem.2014.02.008>
- Barreca S, Velez Colmenares J, Pace A, Orecchio S, Pulgarin C (2015) Escherichia coli inactivation by neutral solar heterogeneous photo-Fenton (HPF) over hybrid iron/montmorillonite/alginate beads. *J Env Chem Eng* 3(1):317–324
- Basumatary KA, Pratim Adhikari P, Ghoshal AK, Pugazhenth G (2016) Fabrication and performance evaluation of faujasite zeolite composite ultrafiltration membrane by separation of trivalent ions from aqueous solution. *Environ Prog Sustain Energy* 35(4):1047–1054. <https://doi.org/10.1002/ep.12325>
- Blanco M, Martinez A, Marcaide A, Aranzabe E, Aranzabe A (2014) Heterogeneous Fenton catalyst for the efficient removal of azo dyes in water. *Am J Analyt Chem* 5(08):490–499. <https://doi.org/10.4236/ajac.2014.58058>
- Cejka J, Zilkova N, Nachtigall P (2005) Molecular sieves: from basic research to industrial applications. In: Proceedings of the 3rd international zeolite symposium (3rd FEZA) Prague, Czech Republic
- de Witte B, van Langenhove H, Demeestere K, Dewulf J (2011) Advanced oxidation of pharmaceuticals: chemical analysis and biological assessment of degradation products. *Crit Rev Environ Sci Technol* 41(3):215–242. <https://doi.org/10.1080/10643380902728698>
- Erdemoglu M, Sarikaya M (2006) Effects of heavy metals and oxalate on the zeta potential of magnetite. *J Colloid Interface Sci* 300(2):795–804. <https://doi.org/10.1016/j.jcis.2006.04.004>
- Fatta-Kassinos D, Meric S, Nikolaou A (2011) Pharmaceutical residues in environmental waters and wastewater: current state of knowledge and future research. *Anal Bioanal Chem* 399(1):251–275. <https://doi.org/10.1007/s00216-010-4300-9>
- Feng J, Hu X, Yue PL, Zhu HY, GQ L (2003) Discoloration and mineralization of reactive red HE-3B by heterogeneous photo-Fenton reaction. *Water Res* 37(15):3776–3784. [https://doi.org/10.1016/S0043-1354\(03\)00268-9](https://doi.org/10.1016/S0043-1354(03)00268-9)
- Ghaly MY, Härtel G, Mayer R, Haseneder R (2001) Photochemical oxidation of P-chlorophenol by UV/ H_2O_2 and photo-Fenton process. A comparative study. *Waste Manag* 21(1):41–47. [https://doi.org/10.1016/S0956-053X\(00\)00070-2](https://doi.org/10.1016/S0956-053X(00)00070-2)
- Ghatak HR (2014) Advanced oxidation processes for the treatment of biorecalcitrant organics in wastewater. *Crit Rev Environ Sci Technol* 44(11):1167–1219. <https://doi.org/10.1080/10643389.2013.763581>
- Hartmann M, Kullmann S, Keller H (2010) Wastewater treatment with heterogeneous Fenton-type catalysts based on porous materials. *J Mat Chem* 20(41):9002–9017. <https://doi.org/10.1039/c0jm00577k>
- Huang W, Luo M, Wei C, Wang Y, Hanna K, Mailhot G (2017) Enhanced heterogeneous photo-Fenton process modified by magnetite and EDDS: BPA degradation. *Environ Sci Pollut R* 24(11):10421–10429. <https://doi.org/10.1007/s11356-017-8728-8>

- Igos E, Benetto E, Venditti S, Kohler C, Cornelissen A, Moeller R, Biber A (2012) Is it better to remove pharmaceuticals in decentralized or conventional wastewater treatment plants? A life cycle assessment comparison. *Sci Total Environ* 438:533–540. <https://doi.org/10.1016/j.scitotenv.2012.08.096>
- Jiang C, Xu Z, Guo Q, Zhuo Q (2014) Degradation of bisphenol A in water by the heterogeneous photo-Fenton. *Environ Technol* 5(8): 966–972
- Kasiri MB, Aleboyyeh H, Aleboyyeh A (2008) Degradation of acid blue 74 using Fe-ZSM5 zeolite as a heterogeneous photo-Fenton catalyst. *Appl Catal B* 84(1):9–15. <https://doi.org/10.1016/j.apcatb.2008.02.024>
- Kim S, Durand P, Roques-Carmes T, Eastoe J, Pasc A (2015) Metallo-solid lipid nanoparticles as colloidal tools for meso-macroporous supported catalysts. *Langmuir* 31(5):1842–1849. <https://doi.org/10.1021/la504708k>
- Klamerth N, Malato S, Agüera A, Fernández-Alba A, Mailhot G (2012) Treatment of municipal wastewater treatment plant effluents with modified photo-Fenton as a tertiary treatment for the degradation of micro pollutants and disinfection. *Environ Sci Technol* 46(5): 2885–2892. <https://doi.org/10.1021/es204112d>
- Kovalova L, Knappe DRU, Lehnberg K, Kazner C, Hollender J (2013) Removal of highly polar micropollutants from wastewater by powdered activated carbon. *Environ Sci Pollut Res* 20(6):3607–3615. <https://doi.org/10.1007/s11356-012-1432-9>
- Kowalska-Kuś J, Held A, Nowińska K (2013) Oxydehydrogenation of C₂–C₄ hydrocarbons over Fe-ZSM-5 zeolites with N₂O as an oxidant. *Catal Sci Tech* 3(2):508–518. <https://doi.org/10.1039/C2CY20536J>
- Kuzniatsova T, Kim Y, Shqau K, Dutta PK, Verweij H (2007) Zeta potential measurements of zeolite Y: application in homogeneous deposition of particle coatings. *Microporous Mesoporous Mater* 103(1):102–107. <https://doi.org/10.1016/j.micromeso.2007.01.042>
- Lam M, Mabury S (2005) Photodegradation of the pharmaceuticals atorvastatin, carbamazepine, levofloxacin, and sulfamethoxazole in natural waters. *Aquat Sci* 67(2):177–188. <https://doi.org/10.1007/s00027-004-0768-8>
- Li Y, Lu Y, Zhu X (2006) Photo-Fenton discoloration of the azo dye X-3B over pillared bentonites containing iron. *J Hazard Mater* 132(2): 196–201. <https://doi.org/10.1016/j.jhazmat.2005.07.090>
- Li L, Shen Q, Li J, Hao Z, Ping Xu Z, Max Lu GQ (2008) Iron-exchanged FAU zeolites: preparation, characterization and catalytic properties for N₂O decomposition. *Appl Catal A: General* 344(1):131–141. <https://doi.org/10.1016/j.apcata.2008.04.011>
- Loaiza-Ambuludi S, Panizza M, Oturan N, Oturan MA (2014) Removal of the anti-inflammatory drug ibuprofen from water using homogeneous photocatalysis. *Catal Today* 224:29–33. <https://doi.org/10.1016/j.cattod.2013.12.018>
- Lutz W (2014) Zeolite Y: synthesis, modification, and properties—a case revisited. *Adv Mater Sci Eng ID* 724248
- Mariangela G, Rizzo L, Farina A (2013) Endocrine disruptors compounds, pharmaceuticals and personal care products in urban wastewater: implications for agricultural reuse and their removal by adsorption process. *Environ Sci Pollut Res* 20(6):3616–3628
- Miralles-Cuevas S, Oller I, Ruiz Aguirre A, Sánchez Pérez JA, Malato Rodríguez S (2014) Removal of pharmaceuticals at microg L⁻¹ by combined nanofiltration and mild solar photo-Fenton. *Chem Eng J* 239:68–74. <https://doi.org/10.1016/j.cej.2013.10.047>
- Natali Sora I, Fumagalli D (2017) Fast photocatalytic degradation of pharmaceutical micropollutants and ecotoxicological effects. *Environ Sci Pollut Res* 24(14):12556–12561. <https://doi.org/10.1007/s11356-016-7640-y>
- Neamu M, Catrinescu C, Kettrup A (2004a) Effect of dealumination of iron(III)-exchanged Y zeolites on oxidation of reactive yellow 84 azo dye in the presence of hydrogen peroxide. *Appl Catal B* 51(3): 149–157. <https://doi.org/10.1016/j.apcatb.2004.01.020>
- Neamu M, Zaharia C, Catrinescu C, Yediler A, Macoveanu M, Kettrup A (2004b) Fe-exchanged Y zeolite as catalyst for wet peroxide oxidation of reactive azo dye Procion Marine H-EXL. *Appl Catal B* 48(4): 287–294. <https://doi.org/10.1016/j.apcatb.2003.11.005>
- Nidheesh PV (2015) Heterogeneous Fenton catalysts for the abatement of organic pollutants from aqueous solution: a review. *RSC Adv* 5(51): 40552–40577. <https://doi.org/10.1039/C5RA02023A>
- Noorjahan M, Durga Kumari V, Subrahmanyam M, Panda L (2005) Immobilized Fe(III)-HY: an efficient and stable photo-Fenton catalyst. *Appl Catal B* 57(4):291–298. <https://doi.org/10.1016/j.apcatb.2004.11.006>
- Oturan MA, Aaron JJ (2014) Advanced oxidation processes in water/wastewater treatment: principles and applications. A review. *Crit Rev Environ Sci Technol* 44(23):2577–2641. <https://doi.org/10.1080/10643389.2013.829765>
- Richardson SD, Kimura SY (2016) Water analysis: emerging contaminants and current issues. *Anal Chem* 88(1):546–582. <https://doi.org/10.1021/acs.analchem.5b04493>
- Rodriguez S, Aurora S, Arturo R (2011) Effectiveness of AOP's on abatement of emerging pollutants and their oxidation intermediates: nicotine removal with Fenton's reagent. *Desalination* 280(1):108–113. <https://doi.org/10.1016/j.desal.2011.06.055>
- Rutkowska M, Chmielarz L, Jabłońska M, Van Oers CJ, Cool P (2014) Iron exchanged ZSM-5 and Y zeolites calcined at different temperatures: activity in N₂O decomposition. *J Porous Mater* 21(1):91–98. <https://doi.org/10.1007/s10934-013-9751-x>
- Sanches S, Rodrigues A, Cardoso V, Benoliel M, Crespo G, Pereira V (2016) Comparison of UV photolysis, nanofiltration, and their combination to remove hormones from a drinking water source and reduce endocrine disrupting activity. *Environ Sci Pollut Res* 23(11): 11279–11288. <https://doi.org/10.1007/s11356-016-6325-x>
- Trapido M, Epold I, Bolobajev J, Dulova N (2014) Emerging micropollutants in water/wastewater: growing demand on removal technologies. *Environ Sci Pollut Res* 21(21):12217–12222. <https://doi.org/10.1007/s11356-014-3020-7>
- Treacy MMJ, Higgins JB (2007) FAU—faujasite. In: Collection of simulated XRD powder patterns for zeolites, Fifth edn. Elsevier Science B.V, Amsterdam, pp 166–167. <https://doi.org/10.1016/B978-044453067-7/50548-7>
- Turapan S, Kongkachuichay P, Worathanakul P (2012) Synthesis and characterization of Fe/SUZ-4 zeolite. *Procedia Eng* 32:191–197. <https://doi.org/10.1016/j.proeng.2012.01.1256>
- Verboekend DN, Nuttens R, Locus J, Van Aelst P, Verolme JC, Groen J, Pérez-Ramírez SBF (2016) Synthesis, characterization, and catalytic evaluation of hierarchical faujasite zeolites: milestones, challenges, and future directions. *Chem Rev* 45(12):3331–3352. <https://doi.org/10.1039/C5CS00520E>
- Xavier S, Gandhimathi R, Nidheesh PV, Ramesh ST (2016) Comparative removal of magenta MB from aqueous solution by homogeneous and heterogeneous photo-Fenton processes. *Desalin Water Treat* 57(27):12832–12841. <https://doi.org/10.1080/194433994.2015.1054887>
- Yue Y, Liu H, Yuan P, Yu C, Bao X (2015) One-pot synthesis of hierarchical FeZSM-5 zeolites from natural aluminosilicates for selective catalytic reduction of NO by NH₃. *Sci Rep* 5(1):09270. <https://doi.org/10.1038/srep09270>